Preparation and characterization of gliadin-based core-shell microcapsules by three antisolvent approaches

Yang, Y., Han, L., Cao, J., Yang, X., Hu, C., Yang, J., Zheng, Q., Zhang, X., Hu, B

Preparation and characterization of gliadin-based core-shell microcapsules by three antisolvent approaches

Yisu Yang, Lingyu Han, Jijuan Cao, Xi Yang, Chuhuan Hu, Jixin Yang, Qiuyue Zheng, Xiaobo Zhang, Bing Hu

PII: S0023-6438(23)01214-8

DOI: https://doi.org/10.1016/j.lwt.2023.115635

Reference: YFSTL 115635

To appear in: *LWT - Food Science and Technology*

Received Date: 24 August 2023

Revised Date: 26 November 2023

Accepted Date: 3 December 2023

Please cite this article as: Yang, Y., Han, L., Cao, J., Yang, X., Hu, C., Yang, J., Zheng, Q., Zhang, X., Hu, B., Preparation and characterization of gliadin-based core-shell microcapsules by three antisolvent approaches, *LWT - Food Science and Technology* (2024), doi: https://doi.org/10.1016/j.lwt.2023.115635.

Preparation and Characterization of Gliadin-based Core-Shell Microcapsules by Three Antisolvent Approaches

Yisu Yang [b †], Lingyu Han [a †], Jijuan Cao [a*], Xi Yang [b], Chuhuan Hu [b], Jixin Yang [c], Qiuyue Zheng [a], Xiaobo Zhang [a], Bing Hu [a*]

[a] Key Laboratory of Biotechnology and Bioresources Utilization of Ministry of Education, School of Life Sciences, Dalian Minzu University, Dalian 116600, China

[b] Department of Food Science and Technology, Tokyo University of Marine Science and Technology, 4-5-7 Konan, Minato-ku, Tokyo, 108-8477, Japan

[c] Faculty of Arts, Science and Technology, Wrexham Glyndwr University, Plas Coch, Mold Road, Wrexham, LL11 2AW, United Kingdom

*Corresponding Authors:

Prof. Jijuan Cao

E-mail: caojijuan@dlnu.edu.cn

Dr. Bing Hu

E-mail: hubing19871121@163.com

† The authors contributed equally to this work.

Abstract: Gliadin, a versatile wheat-derived protein, has great potential in the creation of nanostructured delivery systems for encapsulating various hydrophobic bioactive substances. Despite gliadin's well-established potential in creating nanostructured delivery systems for hydrophobic substances, its utilization for encapsulating hydrophilic compounds remains a relatively unexplored domain. This study investigated the feasibility of preparing gliadin-based core-shell microcapsules using different antisolvent methods and assessed their controlled release capabilities for hydrophilic compounds. It employed three commonly used food polysaccharides, alginate, κ-carrageenan, and agar, as hydrophilic microbeads and selected thiamine and ethyl maltol as model compounds. The microcapsules were constructed by two steps: 1) The microbeads were prepared by a water-in-oil emulsion template under different gelling conditions; 2) The microbeads were dispersed into aqueous ethanol/urea/acetic acid gliadin solutions, during which the slow migration of water from inside the microbeads to the outer gliadin solution decreased the solubility of gliadin and promoted the deposition of gliadin onto the surface of the microbeads, finally leading to the formation of the core-shell structure. The resulting core-shell microcapsules exhibited adjustable particle sizes from 80.0-850.0 μm in diameter and shell thickness ranging from 8.0-30.0 μm. Moreover, the microcapsules exhibited controlled release behavior for hydrophilic compounds, with only 20.0% of thiamine being released after 90 minutes, and this release rate can be finely tuned by controlling the shell thickness. These gliadin-based core-shell microcapsules are considered as promising carriers for the controlled delivery of hydrophilic compounds.

Keywords: Encapsulation; Delivery systems; Hydrophilic compounds; Controlled release.

1. Introduction

Gliadin is the major storage protein present in wheat with good biocompatibility, biodegradability, and nutritional functionality (Song, Sun, Gul, Mata, & Fang, 2021). Structurally, gliadin contains a glutamine- and proline-rich region at its central site and hydrophobic amino acid residues at the terminal domain (Matsushima, Danno, Takezawa, & Izumi, 1997; Patel, 2018). The unique amino acid composition and structural characteristics render gliadin insoluble in water yet soluble in aqueous solutions containing appropriate concentrations of urea, ethanol, or acetic acid (Li, Xia, Shi, & Huang, 2011). In addition, these structural characteristics also allow gliadin to possess typical amphiphilicity and strong ability to self-assemble into micro- or nanostructures for delivering bioactive components (Wang, Geil, & Padua, 2004). At present, increasing attention has been paid to exploit the applicability of gliadin as colloidal delivery systems, with numerous functional compounds being considered, such as drugs (Arangoa, Campanero, Renedo, Ponchel, & Irache, 2001), nutraceuticals, pigments (Balaguer et al., 2014), and flavoring agents (Kasaai, 2018; Patel, Heussen, Dorst, Hazekamp, & Velikov, 2013).

So far, a number of gliadin-based nanostructures (e.g. nanoparticles) have been fabricated and used as food-grade colloidal delivery systems to improve the solubility and stability of the loaded compounds (Joye, Nelis, & McClements, 2015). Gliadin nanoparticles improve the solubility and stability of loaded curcumin (Yang et al., 2021). In addition, encapsulation of bioactive phloretin in gliadin/sodium carboxymethyl cellulose nanoparticles by simple antisolvent precipitation increases its bioaccessibility, by increasing both its water solubility and stability (He et al., 2022). Meanwhile, encapsulation of gum arabic in gliadin-chitosan complexed nanoparticles improves its chemical stability/dissolution and antioxidant activity of resveratrol (Wu et al., 2020).

Generally, gliadin-based nanoparticles have been predominantly employed for encapsulating hydrophobic nutraceutical compounds. Although gliadin nanoparticles have found extensive applications for this purpose, limited information is available concerning the encapsulation of hydrophilic nutraceutical compounds within gliadin-based structures. Recently, the potential of gliadin nanoparticles for the protection and oral delivery of ascorbic acid was demonstrated for the first time (Voci, Gagliardi, Fresta, & Cosco, 2022). Nevertheless, the nanoprecipitation technique employed for these systems is time-consuming, taking approximately 9 hours for preparation of nanoparticles. Hence, there is still an urgent need to develop novel, facile, and scalable techniques for fabricating gliadin-based delivery systems for hydrophilic compounds.

One feasible way is to construct core-shell microcapsules based on gliadin. Core-shell microcapsules generally can combine the advantageous functionality of both the core and shell materials, so that better functionalities such as higher moisture and heat resistance of the microcapsules, good protective effect of the loaded compounds against oxidation, as well as satisfactory masking of unpleasant flavors can be achieved (Hendrickson, Smith, South, & Lyon, 2010; Yu et al., 2018). Due to these advantages, core-shell microcapsules have found wide applications in the fields of material science (Liu, Liu, Ma, Goff, & Zhong, 2020), biomedicine (Martins, Barreiro, Coelho, & Rodrigues, 2014), bioengineering (Kozlowska & Kaczmarkiewicz, 2019), and the culinary industry (He et al., 2018; Hu et al., 2020). Another significant advantage of core-shell microcapsules is that they can exhibit high loading efficiency and more controllable release behavior of the loaded bioactive compounds, a favorable property for improving their bioavailability and physicochemical stability (Botelho, Canas, & Lameiras, 2017). Moreover, the selection of the core and the shell materials may exert a significant effect on the functionality of the microcapsules, indicating that hydrophilic

core and hydrophobic shell microcapsules can be used in encapsulating hydrophilic nutraceutical compounds. However, there is few information available about the preparation and application of the gliadin-based core-shell microcapsules.

In this work, three polysaccharides with different gelling mechanisms, including alginate, κ-carrageenan, and agar, were selected as hydrophilic core microbeads due to their excellent biocompatibility, non-toxicity, and wide accessibility (Hurtado-Lopez & Murdan, 2006). The core-shell microcapsules were constructed by the emulsion template method to induce the polysaccharide-based microbeads under their respective gelling conditions. Then, these hydrophilic microbeads were immersed in aqueous ethanol/urea/acetic acid gliadin solutions, respectively, to produce the antisolvent effect because of the water migration from inside the microbeads to the outer gliadin solutions. Due to the antisolvent effect, the gliadin gradually became insoluble and tended to deposit onto the surface of the microbeads to form gliadin layers, ultimately producing core-shell microcapsules. Subsequently, electronic microscopies including optical microscope, confocal laser scanning microscope (CLSM), and scanning electron microscope (SEM) were used to visualize the microstructures of the core-shell microcapsules. Furthermore, the release behavior of ethyl maltol and thiamine loaded in the microcapsules, which were used as representatives of volatile functional substances and vitamins, respectively, was also measured.

2. Materials and Methods

2.1. Materials

Alginate (G3909401, mannuronate/guluronate ratio ≈ 2.0) and κ-carrageenan (GP-911NF, purity: 90.0%) were purchased from FMC BioPolymer (Billingstad, Norway). Agar (1182GR500, agaropectin/agarose ratio ≈ 1.75) was purchased from Biofroxx

(Einhausen, Germany). The molecular weights (Mw) of alginate, κ-carrageenan, and agar were determined to be 1.38×10^5 Da (alginate), 1.24×10^5 Da (κ-carrageenan), and 5.98×10^5 Da (agar), respectively, by using gel permeation chromatography (GPC) coupled with multi-angle laser light scattering (MALS) (see supporting materials). Gliadin was purchased from Sigma-Aldrich (Shanghai, China). Urea, ethanol, acetic acid, and calcium carbonate were purchased from Sinopharm Chemical Reagent (Shanghai, China). Medium-chain triglyceride (MCT) (Fatty acid composition: C6: ≤ 0.5%, C8: 53%-65%, C10: 35%-45%, others: ≤ 2.0%) was obtained from KLK Oleo (Kuala Lumpur, Malaysia), and ethyl maltol and thiamine were purchased from Macklin Reagent (Shanghai, China). Unless otherwise stated, ultrapure Milli-Q water was used throughout.

2.2. Turbidity

0.1 g gliadin powder was dissolved in 10.0 mL 100.0-1000.0 mL/L ethanol aqueous solution, 1.9-19.4 mol/L urea aqueous solution (19.4 mol/L is the maximum solubility of urea in water at room temperature, 25 ºC), and 100.0-1000.0 mL/L acetic acid aqueous solution with constant stirring at room temperature for 1 h to obtain the 10.0 g/L gliadin solution, respectively. All the solutions were subject to vortex oscillation to achieve satisfactory mixing, after which the solutions were transferred into quartz cells with a 1.0 cm optical path length. A Shimadzu UV-1900 ultraviolet-visible light spectrophotometer (Shimadzu, Tokyo, Japan) was then used to determine the turbidity of all solutions at 500.0 nm. The value of turbidity (τ, cm^{-1}) was calculated by equation (1) (Li et al., 2012):

$$\tau = (1/L) \ln (I_0/I_t) \quad (1)$$

where L is the optical path length, and I_0 and I_t denotes the intensity of incident and transmitted light, respectively. Each sample was determined in triplicate.

148 *2.3. ζ-Potential*

149 A Zetasizer Nano-ZS instrument (Malvern Instruments, Malvern, UK) was
150 employed to measure the ζ-potential of the pure alginate, κ-carrageenan, and agar
151 solutions (1.0 g/L) as well as the ethanol, urea, and acetic acid gliadin aqueous solutions
152 (1.0 g/L) at a wide pH range (1.0 - 5.0), respectively. To prepare the samples, alginate,
153 κ-carrageenan, and agar (1.0 g each) were individually dissolved in 1.0 L of Milli-Q
154 water. Similarly, gliadin (1.0 g) was dissolved in a solution (1.0 L) containing 700.0
155 mL/L ethanol, 12.6 mol/L urea, or 250.0 mL/L acetic acid, respectively. These
156 concentrations of ethanol, urea, and acetic acid were determined based on the optimal
157 initial antisolvent concentrations inferred from turbidity data. Their pHs were adjusted
158 to 1.0-5.0 using NaOH (0.1 and 1.0 mol/L) and HCl (0.1 and 1.0 mol/L).

159 *2.4. Preparation of core-shell microcapsules*

160 The procedure of preparing core-shell microcapsules is schematically illustrated in
161 Fig. 1. First of all, a water-in-oil emulsion template was adopted to generate hydrophilic
162 micro gel beads. For alginate microbeads, 10.0 g aqueous alginate solution (30.0 g/L)
163 containing 50.0 mM/L $CaCO_3$ was prepared, then mixed with 40.0 g MCT containing
164 20.0 g/L L-α-phosphatidylcholine as emulsifier. The emulsion with different droplet
165 sizes was prepared by homogenizing the alginate mixture solution at 350 or 800 rpm
166 for 20 min using a blender (Eurostar 20 Digital, IKA, Staufen, Germany) and 12000
167 rpm (T25 digital ULTRA TURRAX®, IKA, Staufen, Germany) for 3 min, respectively.
168 Subsequently, 10.0 g MCT containing 100.0 mM/L acetic acid was slowly added to the
169 alginate emulsion under a constant stirring at 50 rpm to induce the slow release of Ca^{2+}
170 ions from $CaCO_3$, thereby crosslinking alginate chains to form microbeads. The final
171 pH value of the microbeads was 4.0.

172 Likewise, for preparation of κ-carrageenan microbeads, 10.0 g of 15.0 g/L κ-

carrageenan solution was mixed with 40.0 g MCT containing 20.0 g/L L-α-phosphatidylcholine, followed by stirring the solution at 300 rpm for 20 min to form emulsion. Subsequently, the emulsion was mixed with 8.0 g MCT and 2.0 g KCl solution (2.0 mol/L) under a mild stirring (50 rpm) to prevent the aggregation of the emulsion droplets and to induce the formation of κ-carrageenan microbeads. For agar, the emulsion was prepared by stirring the agar/MCT mixture (10.0 g of 5.0 g/L agar solution + 40.0 g MCT with 20.0 g/L L-α-phosphatidylcholine) at 200 rpm for 20 min at 95 ºC, followed by rapidly cooling the emulsion in an ice bath under a mild stirring of 50 rpm to induce the gelation of agar microbeads.

After the preparation of hydrophilic polysaccharide microbeads, the core-shell microcapsules were generated by dispersing the microbeads into ethanol/urea/acetic acid gliadin solutions, facilitating the deposition of gliadin onto the microbead surfaces through the antisolvent effect. Specifically, for the ethanol antisolvent method, gradient concentrations of gliadin solutions (5.0, 10.0, 20.0, 30.0, and 40.0 g/L) were prepared by dissolving various amounts of gliadin in a 700.0 mL/L ethanol aqueous solution, with a final pH of 4.0. Subsequently, 5.0 g of the prepared polysaccharide gel microbeads were dispersed into 9.0 g of the gliadin solution under constant stirring at 50 rpm for 30 minutes, resulting in a final ethanol concentration of 450.0 mL/L.

For urea and acetic acid antisolvent methods, a similar procedure was applied. In brief, gradient concentrations of gliadin solutions (5.0, 10.0, 20.0, 30.0, and 40.0 g/L) were prepared by dispersing gliadin into 12.6 mol/L urea solution. The final pH was adjusted to 4.0 using 0.5 mol/L HCl. Then, the microbeads were mixed with the aqueous urea gliadin solution to reach 7.8 mol/L urea solution. Similarly, for acetic acid antisolvent precipitation, gliadin was dissolved in 250.0 mL/L acetic acid solution to obtain different gliadin concentrations (5.0, 10.0, 20.0, 30.0, and 40.0 g/L), after which

198 the microbeads were mixed with the gliadin solution to reach a final acetic acid solution
199 of 100.0 mL/L. The decrease in ethanol/urea/acetic acid concentration was considered
200 to lead to the migration of water molecules from inside the microbeads to the gliadin
201 solutions and the deposition of gliadin onto the surface of the microbeads. The prepared
202 hydrophilic polysaccharide microbeads and the core-shell microcapsules were stored in
203 ultrapure Milli-Q water for further characterization.

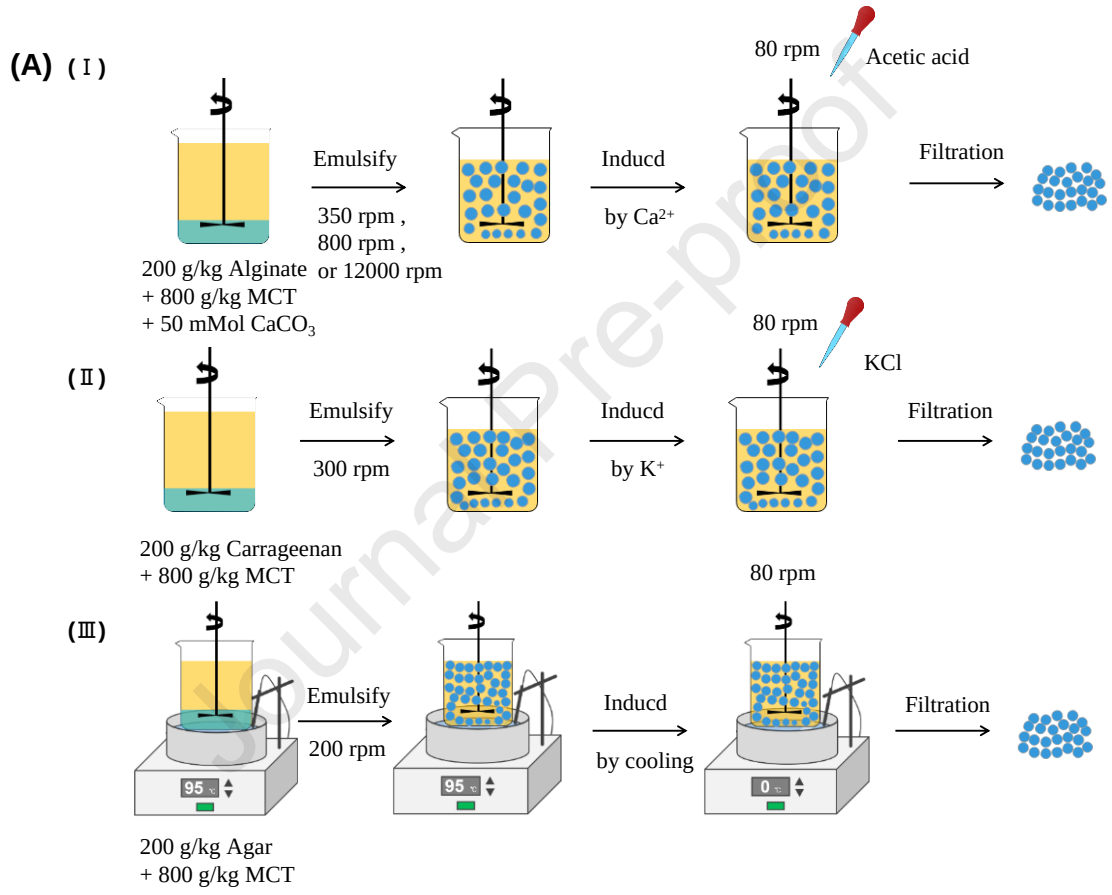

204

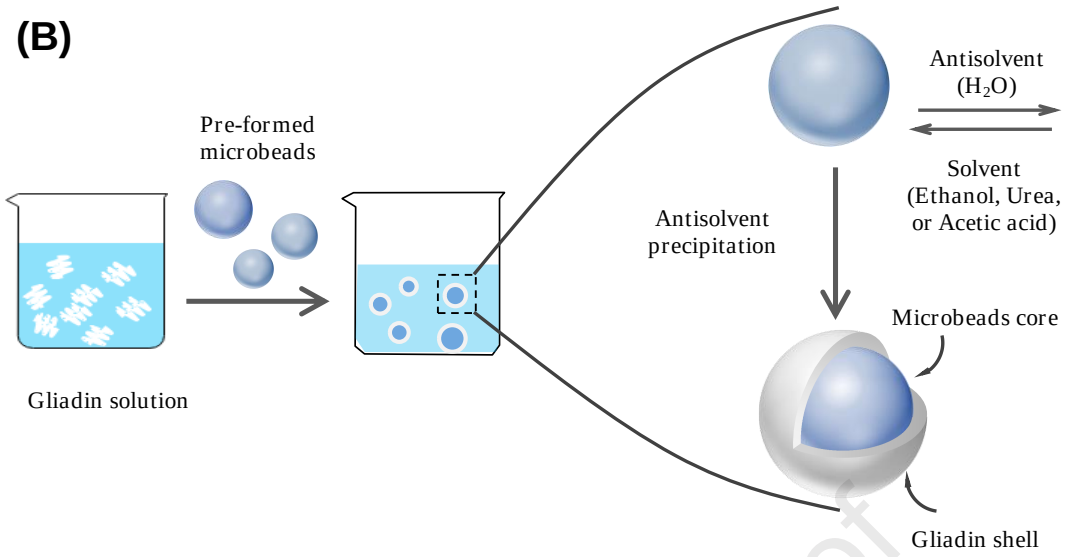

205

206 **Fig. 1.** Schematic diagram of preparation of the microbeads (A) and core-shell
207 microcapsules (B).

208 *2.5. Morphological characterization of core-shell microcapsules*

209 The morphology of the prepared hydrophilic polysaccharide microbeads and the
210 core-shell microcapsules were visualized by microscopes including fluorescence
211 microscope, CLSM, and SEM.

212 The formation of the core-shell structure and the size distributions were evaluated
213 by visualizing light microscopy and fluorescence microscopy of the polysaccharide
214 microbeads and the microcapsules using an IX73 inverted microscope (Olympus,
215 Tokyo, Japan) under a 4× objective with excitation wavelengths of 530-550 nm. 1.0 g
216 microcapsules were stored in 20.0 ml Milli-Q water and stained with 20.0 μL of
217 Rhodamine B (1.0 g/L). Subsequently, Nano Measurer software (v 1.2) was utilized to
218 measure the size distribution of samples for image analysis. To ensure accuracy, a
219 minimum of 100 samples were randomly selected and analyzed during the assessment
220 process.

221 For CLSM observation, the microcapsules were stained by 1.0 g/L of Rhodamine
222 B solution following the same procedure as described above. The microcapsules were

then transferred to a glass slide, covered by a cover slip, and their morphology was observed using a Leica TCS-SP80 CLSM microscope (Olympus, Tokyo, Japan) under fluorescence mode with a 10× objective and an excitation wavelength of 552 nm. The images were then processed using Image J (National Institutes of Health, Bethesda, USA) to calculate the thickness of the shell layer. For the shell thickness of each microcapsule, at least 8 different positions around the boundary of the microcapsule were measured, and for the microcapsules prepared by each strategy, more than 100 microcapsules were measured.

In addition, the surface morphology of both the microbeads and the microcapsules was characterized by SEM (Helios NanoLab G3, FEI, Hillsboro, USA). Briefly, the prepared microbeads and the corresponding microcapsules were immersed in liquid nitrogen to be rapidly frozen, followed by lyophilization at -80.0 ℃ for overnight. After being freeze-dried, microbeads and microcapsules were cut with a microtome to generate cross-sections which were sputtered with a thin gold layer. The morphological images were obtained by visualization using the SEM under high vacuum mode and an accelerating voltage of 15.0 kV.

2.6. Controlled release properties

The ability of the microbeads and the preprepared core-shell microcapsules to controllably release ethyl maltol and thiamine, which were chosen as representative compounds of volatile functional substances and vitamins, respectively, was investigated. Meanwhile, a concentration of 1.0 g/L for ethyl maltol and thiamine was selected to not only ease the investigation of the release rate of the encapsulated materials but also to minimize their impact on the microcapsule preparation process.

For determining the release profile of ethyl maltol, a gas chromatography (GC) system (Agilent 7890B, Santa Clara, USA) was used to quantify the amount of the released ethyl maltol from the microbeads and the microcapsules via a dynamic head-space analysis approach (Chen, Guo, Wang, Yin, & Yang, 2016). The ethyl maltol-loaded microbeads and microcapsules were prepared according to the method described above, with 30.0 g/L alginate stock solution being replaced by 30.0 g/L alginate + 1.0 g/L ethyl maltol solution. When analyzing, 1.0 g of the microbeads and the microcapsules was added to a 100.0 mL airtight bottle to be incubated at 40 °C in dark, respectively. Then, 1.0 mL of the headspace gas was collected by Combi-PAL autosampler (CTC Analytics AG, Zwinger, Switzerland) using a 2.5 mL thermostatic gastight syringe (Hamilton, Bonaduz, Switzerland) at prescribed time intervals (1.5 min) and then injected into Agilent 7890B gas chromatograph (GC) system for detection. The release percentage was calculated by normalization against the equilibrium headspace concentration of 1.0 g of 1.0 g/L ethyl acetate aqueous solution.

For determining the release profile of thiamine, the thiamine-loaded microbeads and the microcapsules were prepared according to a procedure similar to that of the ethyl maltol, with only replacing 1.0 g/L ethyl maltol with 1.0 g/L thiamine. The release profile of thiamine was determined by measuring the UV absorbance of a mixture solution of 1.0 g the microbeads (or 1.0 g the microcapsules) and 10.0 g of deionized water at 246 nm at regular time intervals using a UV-Vis spectrophotometer (TU-1901, Beijing, China). To avoid the degradation of thiamine caused by light exposure, the mixture solution was kept in dark. In the meantime, the absorbance of different concentrations of thiamine dissolved in ultrapure water was also determined to establish a standard calibration curve. The release rate of thiamine from the microbeads and microcapsules was quantified according to Equation (2):

$$Release\ (\%) = 100 \times \frac{At}{Ao} \quad (2)$$

where A_t and A_0 respectively denote the thiamine concentration released at time *t* and the initially encapsulated thiamine concentration.

2.7. Statistical analysis

Each measurement was repeated at least three times, and the results were presented as mean ± standard deviation (SD).

3. Results and discussion

3.1. Solubility of gliadin

Fig. S1 presents the value of turbidity of ethanol/urea/acetic acid aqueous gliadin solutions under different antisolvent conditions. As shown in Fig. S1A, the turbidity of the ethanol aqueous gliadin solution increased as the concentration of ethanol decreased from 900.0 mL/L to 200.0 mL/L. For aqueous ethanol gliadin solution, the significant increase in the turbidity was observed when the concentration of ethanol was reduced to 200.0 mL/L, at which gliadin began to aggregate and precipitate as a result of change of solvent polarity (Kasaai, 2018; Wang & Padua, 2012). As shown in Fig. S1B, a similar trend was observed for the aqueous urea gliadin solution when the concentration of urea was decreased below 15.5 mol/L. When the concentration of urea decreased below 3.9 mol/L, the solution became clear rapidly and gliadin tended to precipitate at the bottom, indicating a steeply decreased solubility of gliadin. In addition, for the aqueous acetic acid gliadin solution, when the concentration of acetic acid decreased from 800.0 mL/L to 200.0 mL/L, the solution was not turbid because gliadin tended to form foamy aggregates which was not diffused. It was the same phenomenon as observed with the urea solutions, only with the "precipitate" less dense than the solution. (Fig. S1C), indicating that acidic acid is more effective at dissolving gliadin than

ethanol (Li et al., 2012).

The determination of turbidity of the gliadin solutions was believed to give an appropriate concentration range of ethanol, urea, and acetic acid in aqueous gliadin solutions for the following preparation of the core-shell microcapsules. It is expected that gliadin preferred to self-aggregate and precipitate in solution if the final concentration of the solvents (ethanol, acetic acid, and urea) was below the lowest concentration threshold. In contrast, at the final concentration above the highest concentration threshold, gliadin preferentially exists as soluble protein in the solutions. In our work, the optimal lowest threshold concentration of ethanol, urea and acetic acid aqueous solutions were identified as 450.0 mL/L, 7.8 mol/L, and 100.0 mL/L, respectively.

3.2. ζ-potential of alginate, κ-carrageenan, agar, and gliadin

As shown in Fig.S2, at pH 1.0-5.0 the three polysaccharides, i.e., alginate, κ-carrageenan, and agar remained negatively charged, and the ζ-potential values of the polysaccharides all increased with increasing pH. In contrast, the gliadin dissolved in aqueous ethanol/urea/acetic acid solutions was positively charged, and the ζ-potential value was significantly affected by the variation of pH. Since gliadin and the polysaccharides exhibited different charge natures, it is believed that the electrostatic attraction would occur between them. In this case, the most significant electrostatic attraction is expected to occur at pH 4.0, at which the electric difference between the positively charged gliadin and the negatively charged polysaccharides is the greatest. Consequently, this kind of electrostatic attraction is considered to favorably contribute to the deposition of gliadin onto the surface of the polysaccharide-based gel bead (Zhang et al., 2021). For acetic acid aqueous gliadin solution, however, the pH value of the solution always remained 0.8, owing to the high acetic acid concentration. The low

pH value may negatively affect the deposition of gliadin onto the surface of the gel beads.

3.3. Morphological characterization of the prepared core-shell microcapsules

3.3.1. Microcapsule size and shell thickness

Fig. 2 presents the particle sizes and morphological images of the prepared core-shell microcapsules. For ethanol system, the alginate microbeads had good ability to be redispersed in solutions and exhibited good transparency (Fig. 2A, Column I), which became opaque after immersing the microbeads in gliadin solution to form core-shell structures because the shell blocked the transmission of light (Fig. 2 A, Column II). The formation of the gliadin shells is believed to occur because of water as antisolvent migration from inside the alginate microbeads to the external gliadin solution, which reduced the concentration of ethanol in gliadin solution and led to an antisolvent effect. In the process, the solubility of gliadin gradually decreased, resulting in its deposition onto the surface of the microbeads to form a dense shell via electrostatic attraction between gliadin and alginate. The fluorescence microscope observation and the CLSM observation of the microcapsules under Fig. 2 A (Columns III and IV) indicated that the microcapsules displayed a clear and uniform shell layer, which again demonstrated the successful production of the core-shell microcapsules. In addition, the alginate microbeads with different particle sizes can be controlled by changing the speed of the homogenizer in the emulsion template method. The particle size of microbeads decreases from 850.0 μm to 80.0 μm as the stirring speed increases from 350 rpm to 12000 rpm (Fig. 2 A). Similarly, the microcapsules can be also generated through the antisolvent effect for the urea and acetic acid system (Fig. 2 B and C). The microcapsules produced by ethanol system were opaquer than those generated by urea and acetic acid systems, indicating the gliadin shell thickness of microcapsules

produced by ethanol system was thicker than the other two. These observations correspond to the turbidity results, where more gliadin nanoparticles precipitated in the ethanol anti-solvent system, resulting in the thicker shell layer.

As shown in Fig. 3, with increasing gliadin concentration, the thickness of the shell layer also increased. For aqueous ethanol and urea systems, a full coverage of the gliadin shell around the surface of the microbeads was observed when 20.0 g/L gliadin solution was used. For the aqueous acetic acid system, a higher concentration of gliadin solution (30.0 g/L) was required to produce a full coverage of the shell. The relatively low efficiency of the acetic acid antisolvent method was assigned to the weaker electrostatic attraction between gliadin and the microbeads and less gliadin nanoparticles precipitate in this method.

The sizes and the shell thickness of the alginate/gliadin-based core-shell microcapsules prepared at different conditions are summarized in Table 1. The mixing or homogenization speed during preparation of the microbeads determined the size of the microcapsules, whose diameter can range from tens to hundreds of micrometers. The shell thickness ranging from 8.0 to 30.0 μm can be tuned by controlling the gliadin concentration and anti-solvent system. For other antisolvent systems, the size and shell thickness of the microcapsules were also adjustable, indicating a good generality of the proposed antisolvent methods for preparing gliadin-based core-shell microcapsules.

Table 1. The size and shell thickness of the alginate/gliadin-based core-shell microcapsules prepared at different conditions.

Anti-solvent System	Gliadin (g/L)	Stirring speed (rpm)	Average particle size (μm)	Average shell thickness (μm)
	10.0	350[I)]	824±14	8.3±0.3
	20.0	350[I)]	828±18	17.7±0.5
Ethanol-Water	30.0	350[I)]	843±15	26.3±0.7

	40.0	350[I)]	846±15	31.7±0.8
	30.0	800[I)]	391±11	18.6±0.5
	30.0	12000[II)]	80±13	12.8±0.6
Urea-Water	10.0	350[I)]	837±15	7.8±0.6
	20.0	350[I)]	839±13	15.5±0.7
	30.0	350[I)]	848±16	22.7±1.2
	40.0	350[I)]	851±17	29.4±0.7
	30.0	800[I)]	352±13	19.8±0.3
	30.0	12000[II)]	114±12	16.7±0.3
Acetic acid System	10.0	350I)	777±16	N/A
	20.0	350[I)]	780±13	N/A
	30.0	350[I)]	785±10	10.3±0.7
	40.0	350[I)]	788±12	17.6±0.4
	30.0	800[I)]	375±14	12.6±0.6
	30.0	12000[II)]	99±9	9.9±0.7

Microcapsules prepared at I) a low speed stirring condition; II) a highspeed homogenization condition. N/A: no data for the thickness of the shell layer because of incomplete coverage.

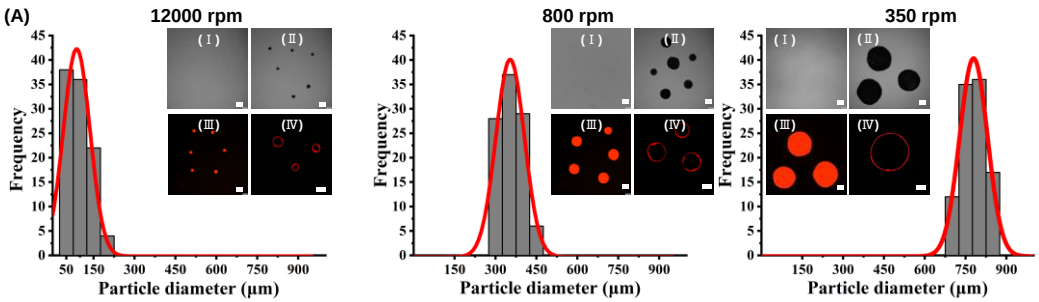

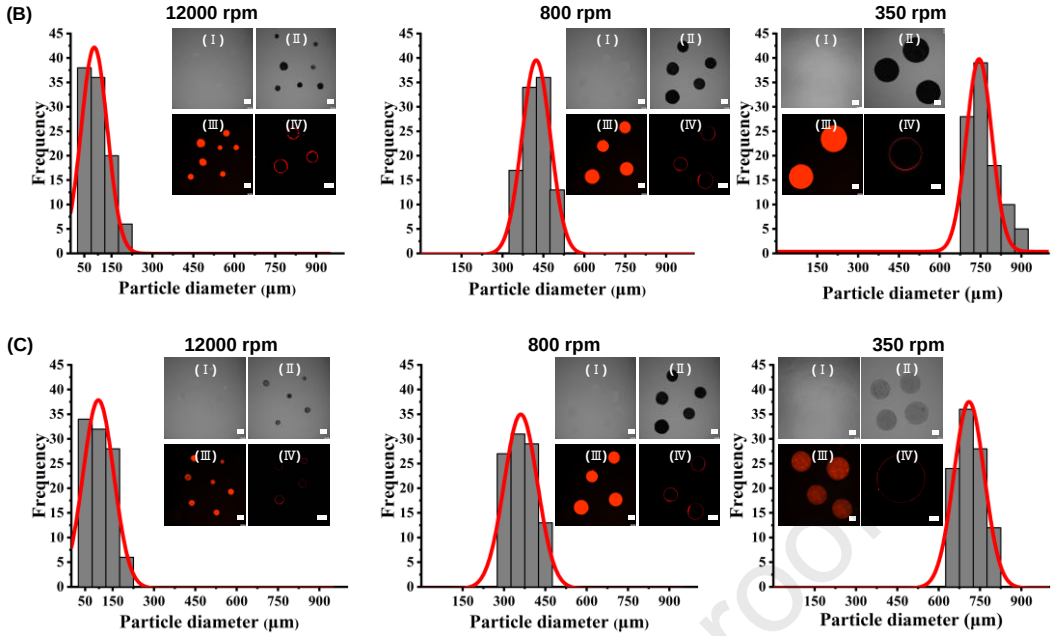

369 **Fig. 2.** The size distributions and morphological characteristics of alginate-gliadin
370 based core-shell microcapsules prepared by (A) ethanol antisolvent system, (B) urea
371 antisolvent system, and (C) acetic acid antisolvent system. Columns I: microbeads
372 without a gliadin shell; Columns II: core-shell microcapsules; Columns III: fluorescent
373 images of these core-shell microcapsules; Columns IV: Confocal laser scanning
374 microscope images of these core-shell microcapsules. Scale bars: 200.0 μm.

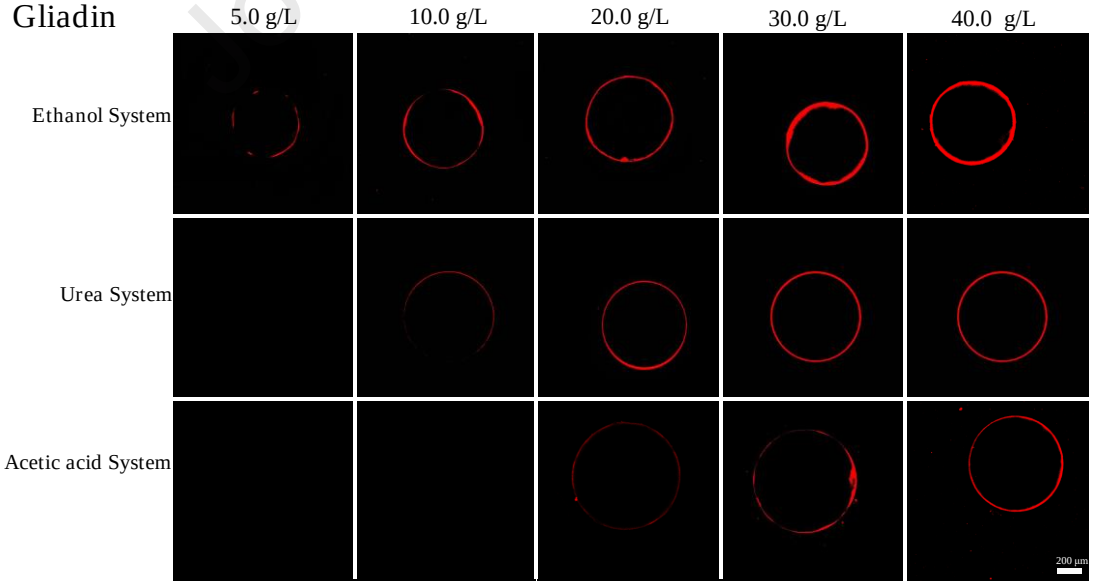

375

376 **Fig. 3.** Confocal laser scanning microscope images of alginate/gliadin core-shell
377 microcapsules prepared by different antisolvent methods and different gliadin

concentrations. Scale bar: 200.0 μm.

3.3.2. Microcapsule morphology

Fig. S3 presents the SEM images of alginate/gliadin core-shell microcapsules. All microcapsules exhibited roughly a spherical shape which was surrounded by a thin layer of smooth shell (Fig. S3, Columns Ⅰ and II), further confirming the formation of core-shell microcapsules. Hydrophilic microbeads exhibited a hollow, porous structure (Fig. S3, Columns Ⅲ), which was attributed to the characteristics of the hydrogel network following freeze-drying and dehydration. This special network structure provided the promise for microcapsules to load bioactive substances.

3.4. Generalization of the tested antisolvent preparation techniques

The results above highlight the ability of these methods to prepare alginate-gliadin core-shell microcapsules with various sizes and shell thicknesses. In these preliminary experiments, alginate was selected as a representative gel owing to its ability to undergo sol-gel transition upon binding to divalent ions (Ca^{2+} ions). To ascertain the broader applicability of these antisolvent methods to diverse gelling polysaccharides, agar was chosen as a representative cold-set gelling polysaccharide to prepare the microcapsules following the same procedure. The bare agar microbeads were transparent under light microscopy (Fig. S4A, Column I), whereas they became opaque after a dense gliadin shell layer was deposited onto the surface of the beads (Fig. S4A, Column II). Fluorescence and CLSM results further confirmed the formation of a uniform, well-defined protein shell (Fig. S4A, Columns III and IV).

Similarly, κ-carrageenan was selected as another representative gelling polysaccharide with special binding capacity to monovalent ions (K^+ ions) to produce the gel beads. As shown in Fig. S5B, the structure of the κ-carrageenan-based

microcapsules paralleled that of alginate- and agar-based microcapsules. Consequently, all three antisolvent methods effectively engendered core-shell microcapsules from distinct initial polysaccharide sources employing varied gelation mechanisms. Therefore, the antisolvent precipitation techniques detailed in this study might be widely applicable to an array of polysaccharides with inherent gelling mechanisms.

3.5 Controlled release properties

Fig. 4 presents the release profiles of ethyl maltol encapsulated inside the alginate microbeads and the alginate/gliadin-based core-shell microcapsules. Ethyl maltol was rapidly released from the alginate microbeads in the initial 5.0 min, followed by a gradual and slow release and finally reached a pseudo-equilibrium after 10 minutes. For the alginate/gliadin-based core-shell microcapsules, ethyl maltol exhibited a similar release profile but with a significant lower release rate than the naked alginate microbeads. In addition, the release rate of ethyl maltol was also dependent on the antisolvent methods, following the order of ethanol < urea < acetic acid. At the equilibrium, the release rate was approximately 80.0% (for the alginate microbeads), 70.0% (acetic acid antisolvent microcapsules), 44.0% (urea antisolvent microcapsules) and 36.0% (ethanol antisolvent microcapsules), respectively. This observed variation in release rates stems from the combined effect of the hydrophilic core and the hydrophobic shell. Alginate microbeads, owing to their small pore size within the gel network, favorably retain ethyl maltol molecules (George & Abraham, 2006). The introduction of a gliadin shell layer further compounded this effect by endowing the microcapsules with a denser microstructure, impeding the migration of ethyl maltol molecules (Hu, et al., 2019). These findings indicated the suitability of the ethanol and urea antisolvent methods in crafting hydrophilic-hydrophobic core-shell microcapsules that adeptly encapsulate and safeguard volatile substances, orchestrating their

427 controlled release for a variety of applications. However, the acetic acid antisolvent
428 method, yielding a thinner gliadin shell, seemed less optimal for achieving controlled
429 release dynamics.

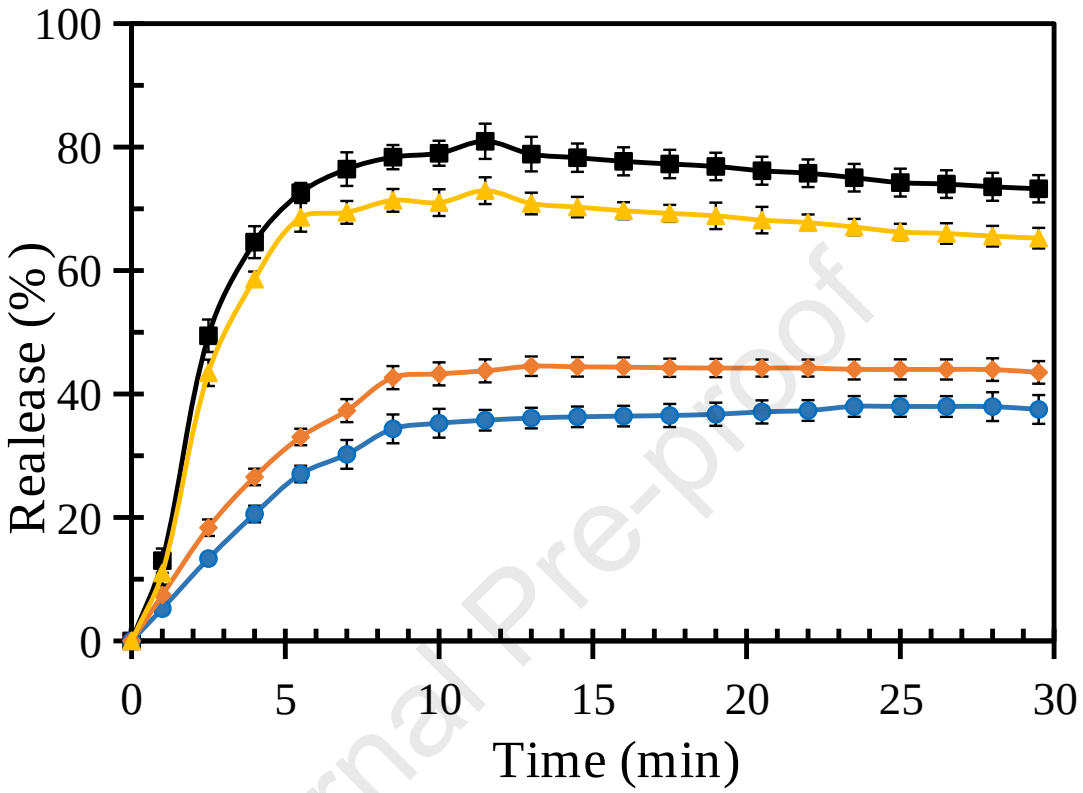

430

431 **Fig. 4.** Release profiles for ethyl maltol-containing alginate microbeads and alginate-
432 gliadin core-shell microcapsules prepared using different antisolvent methods. (■): the
433 alginate microbeads; (●): the core-shell microcapsules prepared based on ethanol anti-
434 solvent; (♦): the core-shell microcapsules prepared based on urea anti-solvent; (▲): the
435 core-shell microcapsules prepared based on acetic acid anti-solvent.

436 To delve deeper into the relationship between shell thickness and controlled
437 release capacity, microcapsules with varying shell thicknesses were prepared for
438 thiamine release. As shown in Fig. 5, for the ethanol antisolvent method, alginate
439 microbeads exhibited swift thiamine release within the initial 15 minutes, with over
440 80.0% released within 60 minutes. In contrast, alginate/gliadin core-shell
441 microcapsules displayed delayed thiamine release, dependent on the gliadin

concentration, with thiamine release amounts of 55.3% for 10.0 g/L gliadin and 30.2% for 20.0 g/L gliadin. As discussed previously, higher gliadin concentrations yielded thicker shell layers, slowing down thiamine diffusion and resulting in a gradual release profile (Li et al., 2021). Similar results were also observed for the alginate/gliadin microcapsules prepared by the urea antisolvent method. However, alginate-gliadin microcapsules generated with the acetic acid antisolvent method, characterized by relatively thin shell layers, displayed limited efficacy in achieving controlled release. This analysis indicated that the manipulation of gliadin shell thickness played a pivotal role, influencing thiamine release kinetics. Notably, in a related study, Juhasz et al. (2021) successfully fabricated liposomal nanocarriers for the controlled release of thiamine, achieving a release rate of 84.0% within 60 minutes. Interestingly, the microcapsules prepared using the ethanol and urea systems exhibited even better controlled release capability when compared to the liposomal nanocarrier approach. These findings exhibited the potential of core-shell microcapsules synthesized through the ethanol and urea antisolvent precipitation methods for effective modulation of vitamin release kinetics. The manipulation of gliadin shell thickness emerged as a pivotal parameter. Consequently, these core-shell microcapsules hold substantial promise for controlled and gradual thiamine release, rendering them suitable for sustained release applications involving food or pharmaceutical compounds.

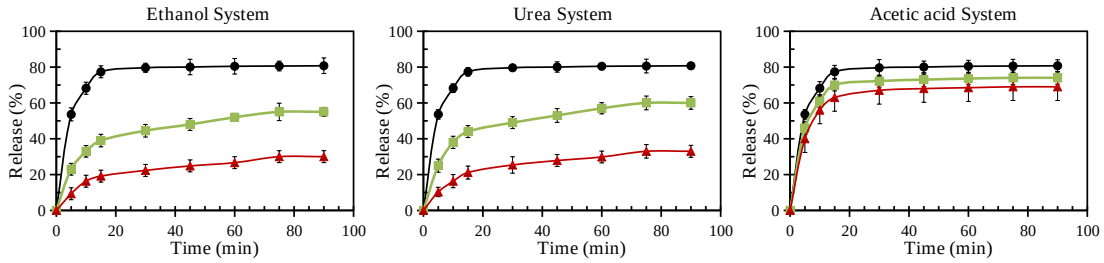

Fig. 5. Thiamine release curves for alginate microbeads and alginate-gliadin core-shell microcapsules produced via the three antisolvent methods with varying shell

464 thicknesses. (●): the alginate microbeads prepared without gliadin; (■): the core-shell
465 microcapsules prepared based on 10.0 g/L gliadin; (▲): the core-shell microcapsules
466 prepared based on 20.0 g/L gliadin.

467 **4. Conclusions**

468 This study significantly advances the application of gliadin-based core-shell
469 microcapsules by demonstrating their efficacy in encapsulating and delivering
470 hydrophilic bioactive compounds, exemplified by ethyl maltol and thiamine. Unlike
471 previous research focusing primarily on hydrophobic substances, this study explores
472 the possibility of using gliadin for hydrophilic encapsulation, broadening its utility and
473 applicability in nanostructured delivery systems. The ability to tailor shell thickness and
474 manipulate release rates offers a versatile platform with profound implications across
475 various industries. In the realm of pharmaceuticals, these microcapsules could
476 revolutionize drug delivery, ensuring precise dosage control and sustaining therapeutic
477 effects. In the food industry, this innovation holds promise for enhancing the stability
478 and bioavailability of hydrophilic nutraceuticals, presenting a novel avenue for
479 functional food development. Moreover, the adaptability of different polysaccharide
480 cores expands the scope of this approach, providing versatility in addressing diverse
481 compound delivery requirements. However, the entrapment efficiency and loading
482 capacity of gliadin-based core-shell microcapsules need further exploration. Overall,
483 gliadin-based core-shell microcapsules transcend the limitations inherent to gliadin
484 nanoparticles in encapsulating hydrophilic bioactive compounds, offering a promise for
485 adoption in biomedical, cosmetic, and culinary domains.

486 **Acknowledgments**

487 This article was supported by National Natural Science Foundation of China (No.

32202232), the National Key Research and Development Project (No. 2021YFF0601900), Liaoning Provincial Science and Technology Innovation Leading Talents Project (No. XLYC2002106), Liaoning Province Livelihood Science and Technology Project (No. 2021JH2/10200019), Department of Education of Liaoning Province (No. LJKZ0037), and Dalian Key Science and Technology Project (No. 2021JB12SN038).

Abbreviations

MCT: Medium-chain triglyceride; CLSM: Confocal scanning laser microscope; SEM: Scanning electron microscopy; GC: Gas chromatograph.

References

Arangoa, M. A., Campanero, M. A., Renedo, M. J., Ponchel, G., & Irache, J. M. (2001). Gliadin Nanoparticles as Carriers for the Oral Administration of Lipophilic Drugs. Relationships Between Bioadhesion and Pharmacokinetics. *Pharmaceutical Research, 18*(11), 1521-1527. https://doi.org/10.1023/a:1013018111829.

Balaguer, M. P., Fajardo, P., Gartner, H., Gomez-Estaca, J., Gavara, R., Almenar, E., & Hernandez-Munoz, P. (2014). Functional properties and antifungal activity of films based on gliadins containing cinnamaldehyde and natamycin. *International Journal of Food Microbiology, 173*, 62-71. https://doi.org/10.1016/j.ijfoodmicro.2013.12.013.

Botelho, G., Canas, S., & Lameiras, J. (2017). Development of phenolic compounds encapsulation techniques as a major challenge for food industry and for health and nutrition fields. *In Nutrient Delivery* (pp. 535-586). http://dx.doi.org/10.1016/B978-0-12-804304-2.00014-7.

Chen, X. W., Guo, J., Wang, J. M., Yin, S. W., & Yang, X. Q. (2016). Controlled volatile release of structured emulsions based on phytosterols crystallization. *Food Hydrocolloids, 56*, 170-179. https://doi.org/10.1016/j.foodhyd.2015.11.035.

George, M., & Abraham, T. E. (2006). Polyionic hydrocolloids for the intestinal delivery of protein drugs: alginate and chitosan--a review. *Journal of Controlled Release, 114*(1), 1-14. https://doi.org/10.1016/j.jconrel.2006.04.017.

He, T., Xu, X., Ni, B., Lin, H., Li, C., Hu, W., & Wang, X. (2018). Metal-Organic Framework Based Microcapsules. *Angewandte Chemie International Edition, 57*(32), 10148-10152. https://doi.org/10.1002/anie.201804792.

He, J., Zhu, J., Yin, S., Yang, X.(2022). Bioaccessibility and intracellular antioxidant activity of phloretin embodied by gliadin/sodium carboxymethyl cellulose nanoparticles. *Food Hydrocolloids*, 122, 107076. https://doi.org/10.1016/j.foodhyd.2021.107076.

Hendrickson, G. R., Smith, M. H., South, A. B., & Lyon, L. A. (2010). Design of Multiresponsive Hydrogel Particles and Assemblies. *Advanced Functional Materials, 20*(11), 1697-1712. https://doi.org/10.1002/adfm.200902429.

Hu, B., Han, L., Ma, R., Phillips, G. O., Nishinari, K., & Fang, Y. (2019). All-Natural Food-Grade Hydrophilic-Hydrophobic Core-Shell Microparticles: Facile Fabrication Based on Gel-Network-Restricted Antisolvent Method. *ACS Applied Materials & Interfaces, 11*(12), 11936-11946. https://doi.org/10.1021/acsami.9b00980.

Hu, Y., Li, C., Wang, J., Jia, X., Zhu, J., Wang, Q., Wang, H., & Yang, Y. (2020). Osmosis manipulable morphology and photonic property of microcapsules with colloidal nano-in-micro structure. *Journal of Colloid and Interface Science, 574*, 337-346. https://doi.org/10.1016/j.jcis.2020.04.062.

Hurtado-Lopez, P., & Murdan, S. (2006). Zein microspheres as drug/antigen carriers: a study of their degradation and erosion, in the presence and absence of enzymes. *Journal of Microencapsulation*, 23(3), 303-314. https://doi.org/10.1080/02652040500444149.

Joye, I. J., Nelis, V. A., & McClements, D. J. (2015). Gliadin-based nanoparticles: Fabrication and stability of food-grade colloidal delivery systems. *Food Hydrocolloids, 44*, 86-93. https://doi.org/10.1016/j.foodhyd.2014.09.008.

Juhasz, A., Ungor, D., Varkonyi, E. Z., Varga, N., & Csapo, E. (2021). The pH-Dependent Controlled Release of Encapsulated Vitamin B(1) from Liposomal Nanocarrier. *International Journal of Molecular Sciences, 22*(18). https://doi.org/10.3390/ijms22189851.

Kasaai, M. R. (2018). Zein and zein -based nano-materials for food and nutrition applications: A review. *Trends in Food Science & Technology, 79*, 184-197. https://doi.org/10.1016/j.tifs.2018.07.015.

Kozlowska, J., & Kaczmarkiewicz, A. (2019). Collagen matrices containing poly(vinyl alcohol) microcapsules with retinyl palmitate – Structure, stability, mechanical and swelling properties. *Polymer Degradation and Stability, 161*, 108-113. https://doi.org/10.1016/j.polymdegradstab.2019.01.019.

Li, C., Fang, K., He, W., Li, K., Jiang, Y., & Li, J. (2021). Evaluation of chitosan-ferulic acid microcapsules for sustained drug delivery: Synthesis, characterizations, and release kinetics in vitro. *Journal of Molecular Structure, 1227*. https://doi.org/10.1016/j.molstruc.2020.129353.

Li, X., Fang, Y., Al-Assaf, S., Phillips, G. O., Yao, X., Zhang, Y., Zhao, M., Zhang, K., & Jiang, F. (2012). Complexation of bovine serum albumin and sugar beet pectin: structural transitions and phase diagram. *Langmuir, 28*(27), 10164-10176. https://doi.org/10.1021/la302063u.

Li, Y., Li, J., Xia, Q., Zhang, B., Wang, Q., & Huang, Q. (2012). Understanding the dissolution of alpha-zein in aqueous ethanol and acetic acid solutions. The Journal of Physical Chemistry B, 116(39), 12057-12064. https://doi.org/10.1021/jp305709y.

Li, Y., Xia, Q., Shi, K., & Huang, Q. (2011). Scaling behaviors of alpha-zein in acetic acid solutions. *The Journal of Physical Chemistry B, 115*(32), 9695-9702. https://doi.org/10.1021/jp203476m.

Liu, H., Liu, F., Ma, Y., Goff, H. D., & Zhong, F. (2020). Versatile preparation of spherically and mechanically controllable liquid-core-shell alginate-based bead through interfacial gelation. *Carbohydrate Polymers, 236*, 115980. https://doi.org/10.1016/j.carbpol.2020.115980.

Martins, I. M., Barreiro, M. F., Coelho, M., & Rodrigues, A. E. (2014). Microencapsulation of essential oils with biodegradable polymeric carriers for cosmetic applications. *Chemical Engineering Journal, 245*, 191-200. https://doi.org/10.1016/j.cej.2014.02.024.

Matsushima, N., Danno, G.-i., Takezawa, H., & Izumi, Y. (1997). Three-dimensional structure of maize a-zein proteins studied by small-angle X-ray scattering. *Biochimica et Biophysica Acta (BBA) - Protein Structure and Molecular Enzymology, 1339*, 14-22. https://doi.org/10.1016/s0167-4838(96)00212-9.

Patel, A. R. (2018). Functional and Engineered Colloids from Edible Materials for Emerging Applications in Designing the Food of the Future. *Advanced Functional Materials, 30*(18). https://doi.org/10.1002/adfm.201806809.

Patel, A. R., Heussen, P. C., Dorst, E., Hazekamp, J., & Velikov, K. P. (2013). Colloidal approach to prepare colour blends from colourants with different solubility profiles. *Food Chemistry, 141*(2), 1466-1471. https://doi.org/10.1016/j.foodchem.2013.03.082.

Song, J., Sun, C., Gul, K., Mata, A., & Fang, Y. (2021). Prolamin-based complexes: Structure design and food-related applications. *Comprehensive Reviews in Food Science and Food Safety, 20*(2), 1120-1149. https://doi.org/10.1111/1541-4337.12713.

Voci, S., Gagliardi, A., Fresta, M., Cosco, D.(2022). Ascorbic acid-loaded gliadin nanoparticles as a novel nutraceutical formulation. *Food Research International*, 161, 111869. https://doi.org/10.1016/j.foodres.2022.111869.

Wang, Q., Geil, P., & Padua, G. (2004). Role of Hydrophilic and Hydrophobic Interactions in Structure Development of Zein Films. *Journal of Polymers and the Environment, 12*(3), 197-202. https://doi.org/10.1023/B:JOOE.0000038552.88467.fc.

Wang, Y., & Padua, G. W. (2012). Nanoscale characterization of zein self-assembly. *Langmuir, 28*(5), 2429-2435. https://doi.org/10.1021/la204204j.

Wu, W., Kong, X., Zhang, C., Hua, Y., Chen, Y., Li, X. (2020). Fabrication and characterization of resveratrol-loaded gliadin nanoparticles stabilized by gum Arabic and chitosan hydrochloride. *LWT - Food Science and Technology*, 129, 109532. https://doi.org/10.1016/j.lwt.2020.109532.

Yang, S., Liu, L., Chen, H., Wei, Y., Dai, L., Liu, J., Yuan, F., Mao, L., Li, Z., Chen, F., & Gao, Y. (2021). Impact of different crosslinking agents on functional properties of curcumin-loaded gliadin-chitosan composite nanoparticles. *Food Hydrocolloids, 112*. https://doi.org/10.1016/j.foodhyd.2020.106258.

Yu, M., Xu, L., Tian, F., Su, Q., Zheng, N., Yang, Y., Wang, J., Wang, A., Zhu, C., Guo, S., Zhang, X., Gan, Y., Shi, X., & Gao, H. (2018). Rapid transport of deformation-tuned nanoparticles across biological hydrogels and cellular barriers. *Nature Communications, 9*(1), 2607. https://doi.org/10.1038/s41467-018-05061-3.

Zhang, X., Hu, B., Zhao, Y., Yang, Y., Gao, Z., Nishinari, K., Yang, J., Zhang, Y., & Fang, Y. (2021). Electrostatic Interaction-Based Fabrication of Calcium Alginate-Zein Core-Shell Microcapsules of Regulable Shapes and Sizes. *Langmuir, 37*(35), 10424-10432. https://doi.org/10.1021/acs.langmuir.1c01098.

Zhang, X., Wei, Z., Wang, X., Wang, Y., Tang, Q., Huang, Q., & Xue, C. (2022). Fabrication and characterization of core-shell gliadin/tremella polysaccharide nanoparticles for curcumin delivery: Encapsulation efficiency, physicochemical stability and bioaccessibility. *Current Research in Food Science, 5*, 288-297. https://doi.org/10.1016/j.crfs.2022.01.019.

Highlights

1) Preparation of novel gliadin-based core-shell microcapsules by antisolvent methods.

2) Adjustable particle sizes and shell thicknesses of core-shell microcapsules.

3) Controlled release of hydrophilic compounds based on these microcapsules.

Declaration of interests

☒ The authors declare that they have no known competing financial interests or personal relationships that could have appeared to influence the work reported in this paper.

☐ The authors declare the following financial interests/personal relationships which may be considered as potential competing interests: